Master's Thesis of Engineering

Elongatable Gripper Fingers with Integrated Stretchable Tactile Sensors for Underactuated Grasping and Dexterous Manipulation

부족구동 파지와 능숙 조작을 위한 유연 촉각센서가 탑재된 길이가 늘어나는 그리퍼

February 2021

Graduate School of Engineering
Seoul National University
Mechanical Engineering Major

Min Sik Choi

Elongatable Gripper Fingers with Integrated Stretchable Tactile Sensors for Underactuated Grasping and Dexterous Manipulation

Advisor Yong−Lae Park

Submitting a master's thesis of Public Administration

October 2020

Graduate School of Engineering
Seoul National University
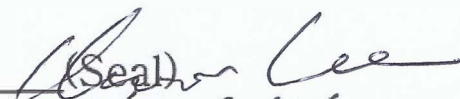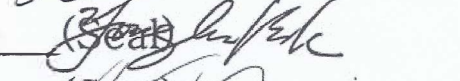Mechanical Engineering Major

Min Sik Choi

Confirming the master's thesis written
by Min Sik Choi
December 2020

Chair	Lee, Kun Woo	(Seal)
Vice Chair	Park, Yong−Lae	(Seal)
Examiner	Cha, Suk Won	(Seal)

Abstract

  The ability to grasp a wider range of objects in size and shape directly relates to the performance of robotic grippers. Adapting to complex geometries of objects requires large degrees of freedom to allow complex configurations. However, complexity in controlling many individual joints lead to introduction of underactuated mechanisms, in which traditional finger designs composed of revolute joints allow only flexion/extension motions. We introduce length-adjustable links in the underactuated finger controlled by an antagonistic tendon pair. The resulting gripper can elongate the fingers for an increased task space or shorten them for improved precision in grasping. For tactile sensing, hyper-elastic soft sensors are used to stretch with the finger elongation. Contact pressures are used as feedback in force control where either the joint angles or the link lengths are adjusted. Lastly, a multimodal control scheme that combines elongation and flexion modes is demonstrated with a task of dexterous manipulation.

i

Table of Contents

Chapter 1. Introduction

Grasping of objects is one of the most essential and vital tasks for dexterous manipulation in robotics. Depending on the design of the robotic gripper, the gripping performance differs based on the diversity of the objects to grasp. Robotic grippers that are able to successfully grasp a wider range of object shapes and sizes are considered to have higher grasping performances than those of conventional grippers with fixed shapes and sizes. Aside from particular gripper applications where the target objects and the manipulation tasks are specified, one general goal of future grippers is to be able to grasp objects with various shapes and sizes with a relatively consistent reliability, of which household items are gaining popularity from increasing interests in human-robot interactions. Ongoing research suggests improving the conformability of the gripper to the target object by increasing the degrees of freedom (DOFs) or by adding compliant mechanisms in the gripper design [1], [2]. Doing so, however, also increases both the complexity and difficulty in modeling and controlling all the DOFs of the gripper [2], [3].

Underactuation provides fewer actuators than the available DOFs of the robot which simplifies the controlling process of the gripper while maintaining the advantage of self-adaptive conformal grasping from the large number of DOFs [4]. For fingered robotic grippers, underactuation causes the gripper fingers to adapt to an arbitrary

shape of the object and distribute the contact forces evenly throughout upon a full grasp without additional complexity in control [5]. The DOFs with active actuation focus on the flexion and extension of the gripper fingers for opening and closing (i.e. grasping and releasing objects), and the other DOFs with unactuation are left to be determined by external constraints acting on the kinetics and the design of the gripper.

Examples of underactuated grippers in the literature are those based on soft or foldable designs [6-9], closed-linkage systems [10-12], or tendon-driven systems [13-20] along with approaches involving geometrical modeling [21-26]. Among these, soft or foldable designs for grippers are difficult to model geometrically because these designs provide an infinite number of DOFs. While grippers that use closed-linkage systems are easier to model, they require predetermined link lengths in design that limit the range of grasp. Tendon-driven designs, however, can be modeled with geometry relatively easily and also do not pose restrictions on the gripper link lengths.

Since tendons typically provide only a unidirectional force, antagonistic tendon routing designs are commonly used [27], [28]. In underactuated gripper finger designs, two tendons as an antagonistic pair actuate up to two DOFs, one of which is primarily for bending motions (i.e. flexion and extension) while the other is either unused or used to control another parameter, such as stiffness [29-33] or length [34]. Providing length control is advantageous in

applications where increasing the robot task space is important for performance in grasping various objects [35-38]. Particularly for gripper applications, using an antagonistic tendon-driven mechanism to control both bending motions and finger lengths is an attractive approach to improve the range of graspable object sizes. Despite the grasping performance advantages gained from elongatable finger designs, there is yet to be an underactuated gripper that actively controls its finger lengths using an antagonistic tendon system.

Aside from the gripper design, the grasp performance improves drastically with the presence of tactile sensors providing information on contact forces. Tactile sensors are useful for feedback control of grasping force [39], [40], object identification [41], [42], and slip detection [43], [44] which help in determining a proper grasp. Traditional robot grippers have fingers that are fixed in length and use tactile sensors that do not need to be stretchable [39], [41]. However, for a gripper where the fingers are designed to be elongatable, integrated tactile sensors need to be stretchable or extendable to match the elongated lengths of the fingers.

Interests in soft robotics have led to research that proposes use of soft, hyper-elastic materials, such as silicone rubbers, to replace traditional rigid materials used in robotics [45]. Specifically, sensors that are fabricated using such soft, hyper-elastic materials have been shown to function at high strain rates up to 250% [46]. By using a liquid conductor in microchannels embedded in a silicone rubber layer, the sensor is able to function properly as a tactile pressure

sensor even while highly stretched [47-50]. These soft, hyper-elastic sensors are therefore suitable to be integrated with elongatable gripper fingers, providing tactile information while still permitting active finger length control.
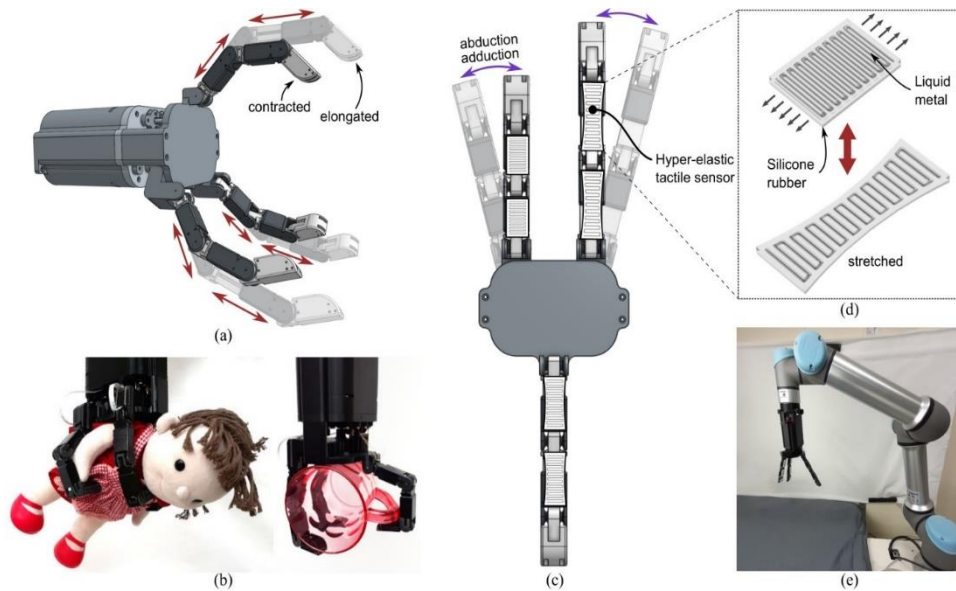
Fig. 1. (a) Finger length configurations showing the contracted and elongated states. (b) Underactuated grasping of objects with non-uniform surfaces. (c) Hyper-elastic tactile sensors integrated with the gripper fingers. Abduction and adduction motions made by the two adjacent fingers. (d) Soft sensor composed of silicone rubber with embedded microchannels filled with liquid metal remains functional while stretched. (e) Gripper attached to the end-effector of a commercial robot arm (Universal Robots, UR5).

In this paper, we present an underactuated tendon-driven robotic gripper design that can simultaneously control both the bending angles and the lengths of the fingers integrated with highly stretchable soft tactile sensors [see Fig. 1(a), (b), and (c)]. Our proposed gripper has three fingers, each of which is actuated by pulling an antagonistic pair of tendon cables for flexion/extension and elongation/contraction motions. The finger is a serial open chain that consists of revolute-prismatic modules with a compression spring at every prismatic joint to maintain the tension in the two tendon cables. For a chain that has more than one module, the system effectively becomes underactuated as the DOFs in the finger exceed the two actuated DOFs by the two tendons. A geometric model is presented to relate the tendon length inputs to the finger lengths and bending angles, which is used in controlling the configurations of the gripper.

Soft sensors on each finger module provide contact information and are made of a hyper-elastic material embedded with microfluidic channels filled with a liquid conductor [see Fig. 1(d)]. The high stretchability of the soft sensors allows them to consistently function as tactile sensors whether the finger is elongated or contracted. Tactile information obtained from the integrated soft sensors provide force feedback to the gripper for closed-loop control.

We demonstrate that one of the elongated and the contracted finger states outperforms the other in grasping performance depending on the size and the shape of the target object. Since the lengths of our gripper fingers are controllable, the best-performing finger lengths

may be chosen based on the dimensions of the target object in application. Using contact force information from the integrated tactile sensors, control schemes that maintain the setpoint contact pressure by adjusting either the grasping angles or the lengths of the fingers are demonstrated through grasping of a balloon that dynamically changes its size. Finally, the flexion and elongation modes of the finger are combined in a multimodal control scheme for a bottle−cap opening task to demonstrate dexterous gripper manipulation.

Chapter 2. Elongatable Finger

2.1. Design of Elongatable Finger Module

Traditional robot gripper fingers are designed as a serial chain of revolute joints with fixed link lengths. Grasping motions of such grippers are combinations of rotation motions made by the revolute joints in the fingers. Their resulting task spaces are limited to the combined spaces of the fingers, which are spheres of radii that are equal to the sums of the finger link lengths. To increase the gripper task space, we propose an elongatable finger design that permits variable finger link lengths by adding prismatic joints between the revolute joints in the serial chain. Each part of the chain then consists of an elongation region from the prismatic joint and a flexion region from the revolute joint [see Fig. 2]. With the addition of the prismatic joints, the task space sphere of each finger increases in radii as much as the sum of the elongated ranges of the prismatic joints.

Adding a prismatic joint to every link in the traditional robot finger, however, increases the number of DOFs to nearly double the original amount. While larger DOFs allow the finger to better conform to object surfaces with arbitrary shapes, they also increase the complexity not only in the physical system but also in control.
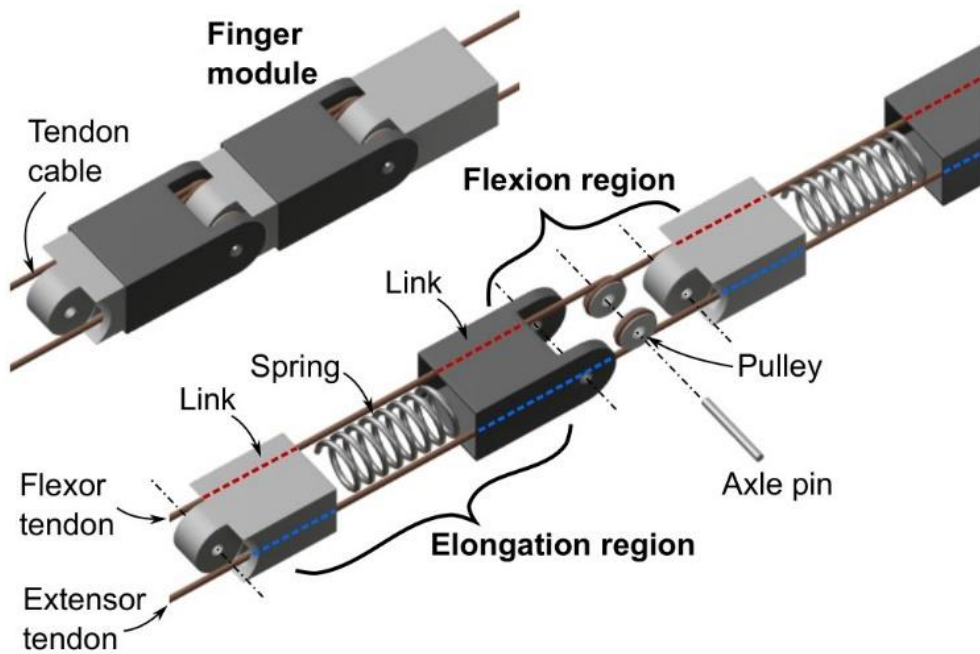
Fig. 2. Gripper finger as a serial chain of pulley－tendon－spring modules with elongation regions at rectangular prism slots and flexion regions at pulleys as prismatic and revolute joints respectively.
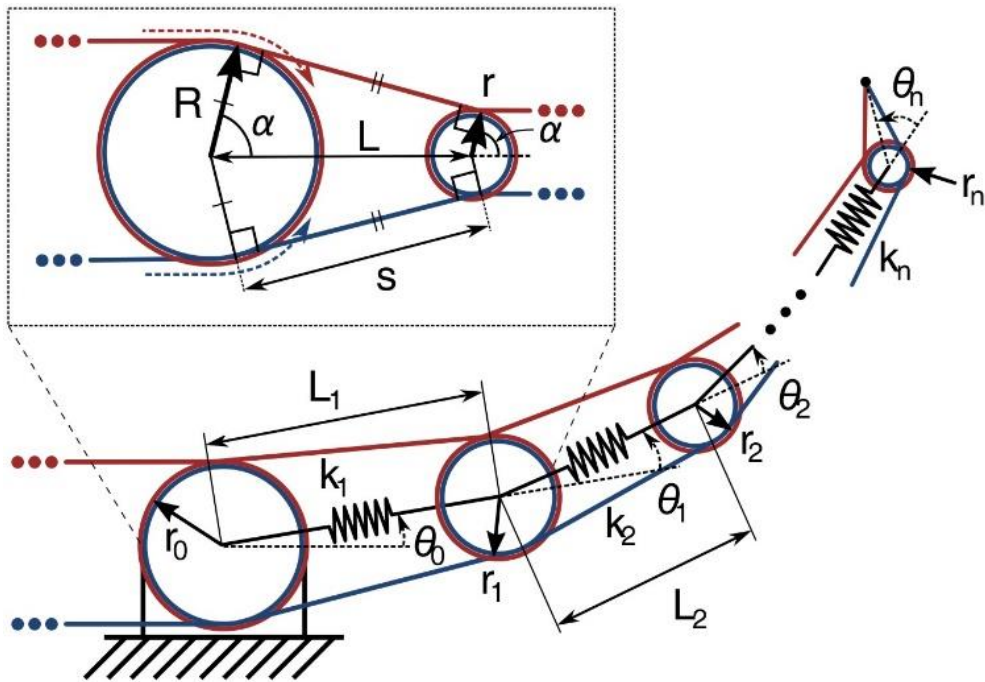
Fig. 3. Schematic drawing of a single finger module with arbitrary pulley radii r and R at a link length distance L.

As is with other grippers that use large or infinite DOFs in the design, our finger uses an underactuation mechanism to simplify the gripper control while maintaining the advantage of having an increased task space. Each finger has two cables routed as an antagonistic tendon pair that controls bending motions (flexion and extension) and lengthening motions (elongation and contraction). The main control parameters of the finger are the joint angles and the link lengths [see Fig. 3]. Specifically, the sum of the joint angles and that of the link lengths of the finger are controlled in our design, leaving the individual joint angles and the link lengths to be determined from underactuation by the object shape or the external constraints in the environment. Only the two tendons of the finger are actuated, providing only two actuated DOFs for each finger regardless of the number of revolute−prismatic modules in the finger.

Depending on the cable lengths of the antagonistic tendon pair, the finger can make both flexion and elongation motions [see Fig. 4]. Since the serial revolute−prismatic chain is repetitive, the finger design can be seen as modular such that one module consists of a revolute−prismatic joint pair. In design, the revolute joint is a frictionless pulley with negligible inertia and the prismatic joint is a frictionless uniaxial rectangular prism slot. The antagonistic tendon pair begins at the most proximal phalanx module of the finger, is kept tight while passing through the rectangular prism slots, wound around each pulley, and anchored at the axis of the pulley of the most distal phalanx that has a negligible radius [see Fig. 3]. One of the tendon

cables is always kept to the lower side of the pulleys (extensor tendon) while the other is always kept to the opposite upper side (flexor tendon) to form an antagonistic pair [see Fig. 2 and Fig. 4]. A compression spring located inside each of the rectangular prism slots prevents slack by maintaining the tension of the tendons. Tendons are actuated by pulling or releasing them, effectively reducing or increasing the lengths. The finger is therefore designed as a serial chain of pulley−tendon−spring modules with two cables in an antagonistic tendon pair that control the joint angles and the link lengths.

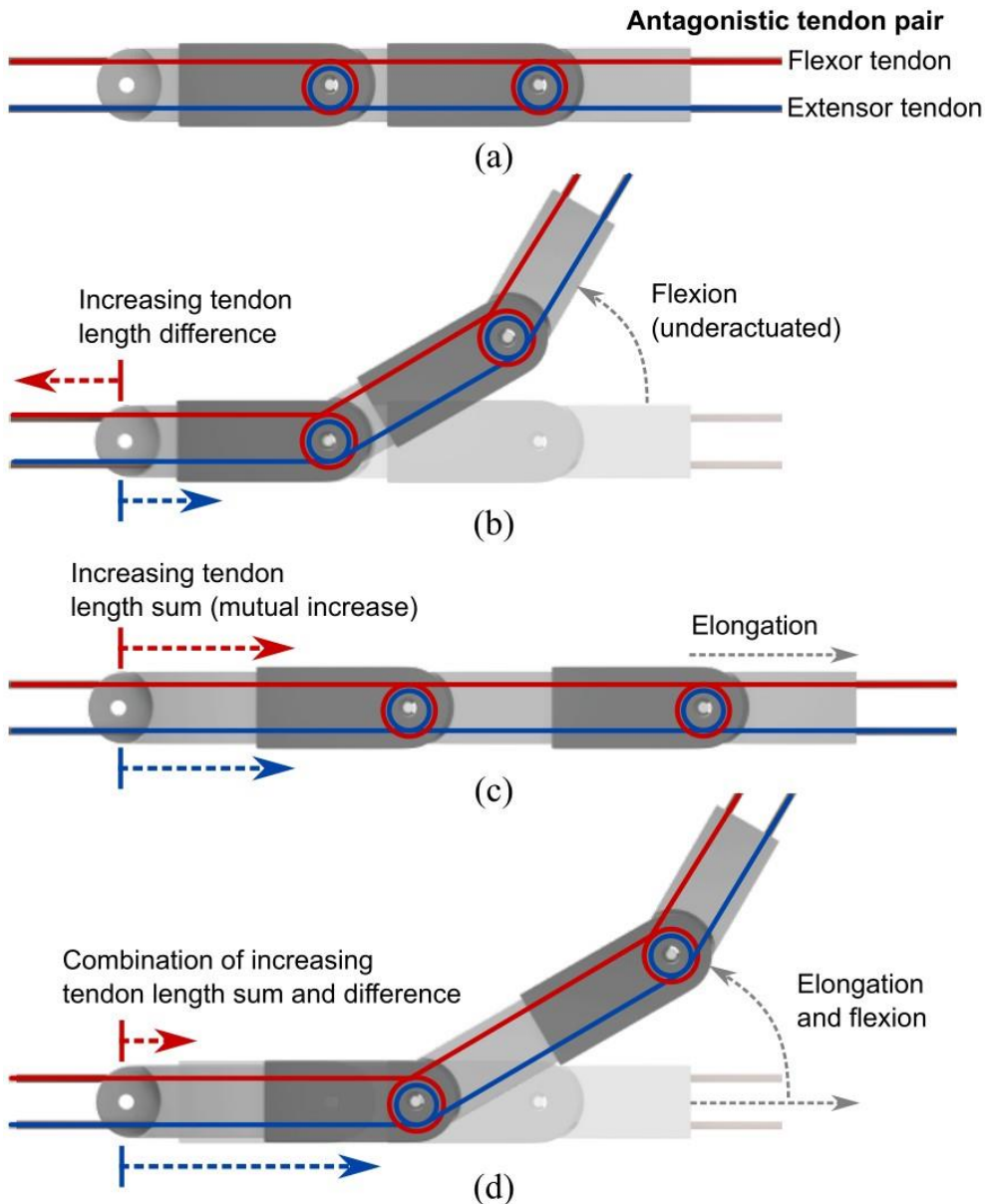**Fig. 4.** (a) Antagonistic tendon pair with the upper cable as the flexor tendon and the lower cable as the extensor tendon. (b) Flexion and extension motions resulting from opposing changes in tendon lengths. (c) Elongation and contraction motions resulting from mutual changes in tendon lengths. (d) Combined flexion and elongation motions resulting from the superposition of tendon length changes.

2.2. Modeling of Finger Module

Assuming the tendon cables are inextensible and negligibly thin, the underactuated elongatable finger can be modeled using a geometric approach. Compression springs only serve to maintain the tension of the tendons and do not provide any geometrical constraints. Geometrical relations required for modeling are sufficiently provided by the pulleys and the tendons. Tendons are wound around the pulleys in the opposite directions as an antagonistic pair. For the simplicity of the geometric model, the pulleys are assumed to be uniform circles and the tendons are assumed to be wound around the pulleys with a small number of turns enough to make sure that the tendons always form tangents with the pulley geometry.

The inset of Fig. 3 illustrates the model of one generic finger module. From similar angles in the model geometry, the angle α at which the tendons leave the previous pulley circle and enter the next circle is found using the four-quadrant arctangent function arctan2(y,x) as

$$\alpha = arctan2(s, R - r) \tag{1}$$

where tangent tendon length s is related to the link length L and the pulley radii r and R as

$$s = \sqrt{L^2 - (R - r)^2} \tag{2}$$

From the above relations, the joint angles and the link lengths of the geometric model of an arbitrarily long serial chain of the pulley-tendon-spring finger module can be related to the tendon lengths. The total length of the extensor tendon and flexor tendon

passing through n number of modules is

$$L_{tendon,extensor} = \sum_{i=1}^{n} s_i + \sum_{i=0}^{n} r_i\left(2\pi + \left(\pi/_2 - \alpha_i\right) + \theta_i\right) \qquad (3)$$

and

$$L_{tendon,flexor} = \sum_{i=1}^{n} s_i + \sum_{i=0}^{n} r_i\left(2\pi + \left(\pi/_2 - \alpha_i\right) + \theta_i\right) \qquad (4)$$

respectively, where individual tangent angle α_i is

$$\alpha_i = arctan2(s_{i+1}, r_i - r_{i+1}) \qquad (5)$$

and individual tangent tendon length s_i is

$$s_i = \sqrt{L_i^2 - (r_i - r_{i-1})^2} \qquad (6)$$

and other notations match those on the left column in Fig. 3.

The two tendon lengths in (3) and (4) show similar terms, some of which have the same sign while others have opposite signs. Linearly combining these two equations by adding and subtracting provides the following two relations:

$$L_{tendon,extensor} + L_{tendon,flexor}$$

$$= 2\sum_{i=1}^{n} s_i + 2\sum_{i=0}^{n} r_i\left(2\pi + \left(\pi/_2 - \alpha_i\right)\right) \qquad (7)$$

$$L_{tendon,extensor} + L_{tendon,flexor} = 2\sum_{i=0}^{n} r_i\theta_i \qquad (8)$$

From observation, the sum relation in (7) depends only on the link lengths and is independent of the joint angles while the difference relation in (8) depends only on the joint angles and is independent of the link lengths. Consequently, the sum and the

difference of the tendon length provide a means of decoupling the control of the finger length and angle.

The difference relation has a clear relation to the sum of the joint angles, which is a desirable and intuitive control parameter. On the other hand, while the sum relation is fully decoupled, it does not have a clear intuitive relation to the link lengths.

A special case that simplifies (7) such that a desirable and intuitive relation to the link lengths is obtained occurs when all the pulleys have the same radii. In this case, the four-quadrant arctangent no longer depends on the link lengths, and the tangent tendon lengths simply become the link lengths. Finger configuration is then described with

$$\sum_{i=1}^{n} L_i = \frac{L_{tendon,extensor} + L_{tendon,flexor}}{2} - 2\pi n r \qquad (9)$$

$$\sum_{i=0}^{n} \theta_i = \frac{L_{tendon,extensor} + L_{tendon,flexor}}{2} \qquad (10)$$

whereby the sum of the link lengths and the sum of the joint angles are clearly controlled by the sum and the difference of the tendon cable lengths. Using these two constraints, the two actuated DOFs are able to control the finger configuration through the sums of the lengths and angles; individual joint angles and link lengths are left to be determined by the external constraints as a result of underactuation.

However, in the general case where pulley radii differ, the pulley radii become the coefficients of the individual joint angles in the tendon length difference relation. Although the individual joint angles are not determined, the pulley radii act as weights that affect how much of the tendon length difference the respective joint occupies per unit angle. Correct design of the pulley radii therefore will have an influence on the behavior of the individual joint angles.

Analogously, the individual link lengths also have a weight factor that is not revealed by the geometric model. Using a static model that considers the tension of the tendon and the compression forces of the spring shows that the stiffnesses k_i of the springs between the revolute joints act as the weights of the individual link lengths for distributing the tendon length sum, especially in the special case when the pulley radii are the same. By using the same pulley radii and the same spring stiffnesses for all modules, equal weights are given to the individual link lengths and joint angles.

2.3. Finger Manufacture and Assembly

To confirm the geometric model, a finger prototype was fabricated consisting of two elongatable modules as the proximal and the middle phalanges and the third link of fixed length as the most distal phalanx (i.e. fingertip). The finger consists of five links, two springs, three axle pins, six pulleys, two tendon wires, and three printed circuit boards (PCBs) for reading the sensor signals. The links and pulleys were made of an acrylic resin (Veroblack Plus, Stratasys) by a 3D

printer (Objet 30, Stratasys). The axle at each revolute joint is a metal pin with a diameter of 0.8 mm. Springs placed at each prismatic joint have stiffnesses of 0.429 N/mm and are 20 mm in length when unloaded and 5 mm when fully compressed. A fishing line (Ultra P.E Line Kevlar, AQUA-X) that has high abrasion resistance and a tensile strength rating of 24 kg was used for the tendon cables. Communication lines of the PCBs attached to the bases of the links were electrically connected to each other through flat flexible cables (FFC) that passed through the centers of the rectangular prism slots and compression springs.

2.4. Gripper Assembly

Three elongatable fingers were assembled to a flat platform to form a palmed gripper with seven actuated DOFs, two for actuation of each finger and one for the abduction/adduction motions. Two adjacent fingers are connected by two smoothly interlocking gears printed by a 3D printer (Objet 30, Stratasys). One of the two gears was connected to a motor shaft while the other was connected to a freely rotating axle made of a metal rod, 2 mm in diameter. The third finger was placed in an opposite manner to be a thumb. Tendon cables from the fingers were tied and wound with multiple turns around the motor shafts assembled to the wrist of the gripper underneath the palm. For motor control, four custom-designed motor driver boards were installed under the seven 12 V direct-current (DC) gear motors.
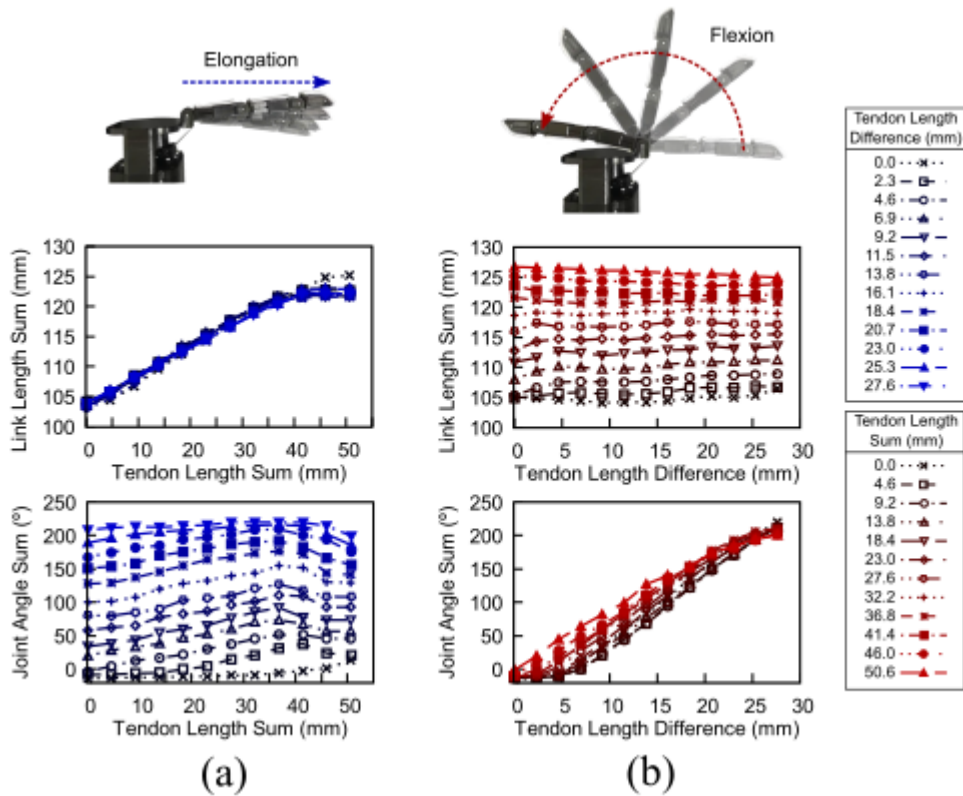
Fig. 5 (a), (b). Graphs in the columns (a) and (b) show the finger configurations according to tendon length sum and difference, respectively.
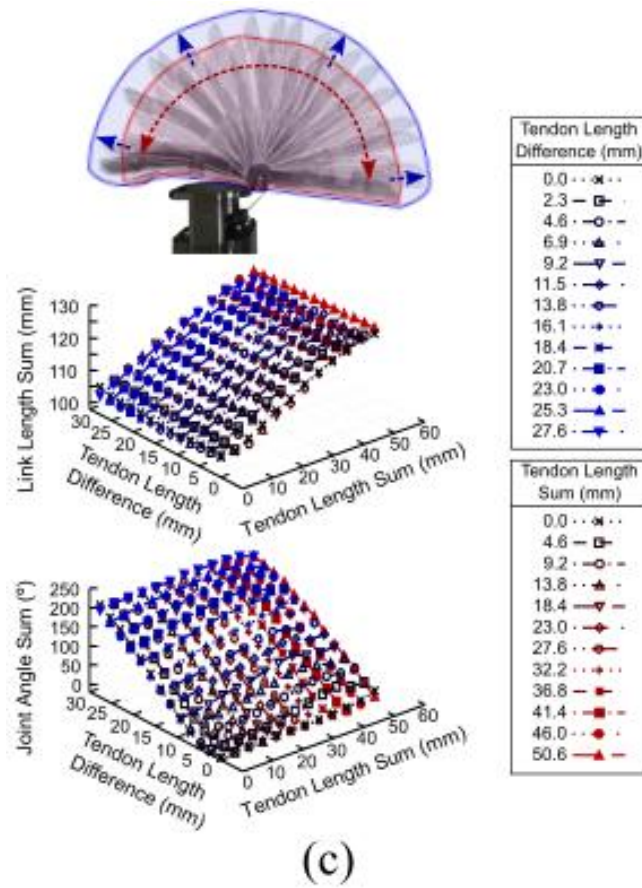
Fig. 5 (c).　Graphs in the column (c) are the respective three−dimensional plots from combining the results in (a) and (b).

2.5. Finger Characterization and Actuation

Characterization was done by attaching the assembled gripper to the end-effector of a commercial robot arm (UR5, Universal Robots). The two tendons of the finger were wrapped around a 12 V DC motor shaft of 3 mm diameter with an in-built rotary encoder of a resolution of 5462 bits per motor shaft revolution. After winding, the motor diameter measured to be 4 mm due to the thickness of the Kevlar tendon cables. The motor shaft position was internally controlled using a proportional-integral-differential (PID) control with the feedback from the encoder.

Encoder values were set to zero in the fully extended and elongated finger position aligning with the gravity vector. Changes in the motor positions reflected by the encoder were linearly mapped to the tendon length changes using the arc lengths. An optical camera (Galaxy A20, Samsung) was used to track the shape and the position of the finger, and an inbuilt accelerometer was used to orient the camera to be perpendicular to the floor plane and parallel to the gravity vector. The end-effector of the robot arm was configured to orthogonal orientations using the inbuilt solver. In Fig. 5, the gripper is oriented parallel to the floor such that gravitational forces do not affect the gripper joint angles. A computer was used to control the motor to move to designated encoder positions whereby a camera snapshot was taken after a sufficiently long settling time for tracking analysis.

Motor positions were changed according to the tendon length sum

and differences as obtained from the geometric model. The first set of images was taken by first fixing the tendon length difference before incrementing the tendon length sum, while the next set was taken by first fixing the tendon length sum and incrementing the tendon length difference [see Fig. 5]. Each resulting snapshot image was tracked at the locations of the axle pin of the motor pulley to provide the joint angles and the link lengths. The tracked positions were calibrated to millimeter length units using the calibration snapshot images of a steel ruler.

As predicted by the geometric model, the characterization results in the left column in Fig. 5 show a strong dependence of the link length sum to the tendon length sum and a weak dependence for the joint angle sum. Similarly, there is a strong dependence of the joint angle sum to the tendon length sum and a weak dependence for the link length sum as shown in the middle column. The resulting plane surfaces by combining the two sets of data as shown in the right column indicate the controllable region of our pulley−tendon−spring finger. With our elongatable finger design, the reachable task space enlarges.

Chapter 3. Stretchable Tactile Sensor

The grasping performance of the gripper improves significantly when tactile sensors are used. Measuring the contact force provides not only force feedback information in closed-loop control but also information on the object and the grasping state, all which are useful in increasing the success of the grasp. Traditional robot grippers are designed with links that do not change in length and therefore are compatible with common tactile sensors that are not highly stretchable. Such tactile sensors are not fully compatible with our elongatable gripper fingers, however, since they either fail to properly cover the entire lengths of the finger links or fail to function properly at high strains resulting from finger elongation.

However, soft sensors with stretchable design that uses a hyper-elastic silicone rubber material with embedded liquid metal microchannels for pressure detection are able to simultaneously elongate with the fingers without any functional failure and also covering the entire finger link length. Pressure and strains are detectable by changes in the electrical resistance of the liquid metal which result from deformations of the microchannel patterns caused by external stimuli. Soft tactile sensors that we have fabricated are designed to function at strains up to 100%. The longer finger elongations are achievable, the higher strains the sensor is able to withstand.
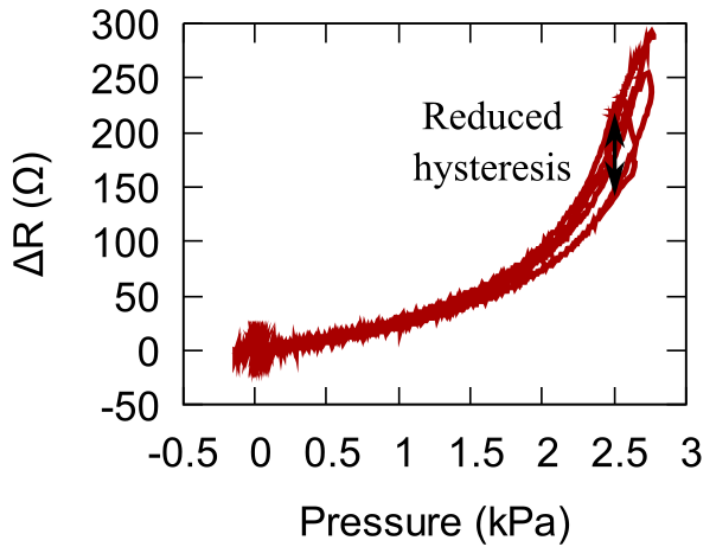
3.1. Sensor Fabrication

For the tactile sensors, silicone rubber (Ecoflex 00-30, Smooth-On) was mixed with a curing agent and a white pigment with a ratio of 1:1:0.1 then degassed in a vacuum chamber. The mixture was poured on a spin-coater and spun at 500 rpm to a thickness less than 1.5 mm. After curing in a thermal convection oven at 60°C for an hour, a pneumatic dispenser (SuperΣCMIII-V2/V5, Musashi Engineering Inc.) was used to draw microchannels on the cured silicone surface with a liquid metal (eutectic gallium-indium or EGaIn) [51]. The same uncured silicone rubber mixture was poured on top of the microchannels and cured, reaching the final thickness of approximately 2.4 mm. An ultra-thin-walled needle with an outer diameter of 0.20 mm was used to inject additional EGaIn into the microchannels to prevent disconnections when stretched or pressed excessively. This step also reduced hysteresis which was evaluated by increasing and decreasing pressure repeatedly: depending on whether the pressure is loading or unloading, the sensor signal responding to the same pressure is different, since the viscoelasticity of the polymer causes time delay for the EGaIn inside to recover its deformation after loading of pressure. However, after additional EGaIn was reinjected, the pressure in the microchannels increased, reducing the time delay and hysteresis consequently [see Fig. 6]. Thin copper wires were then inserted into the ends of the channel path for electrical connection, and a small amount of adhesive (Sil-Poxy, Smooth-On) was applied on top to anchor the wires. U-

shaped snap-fit anchors were fabricated using a 3D printer (Objet 30, Stratasys) and were glued on opposite ends of the sensor using a cyanoacrylate adhesive (Axia 1500, Axia) [see Fig. 7].
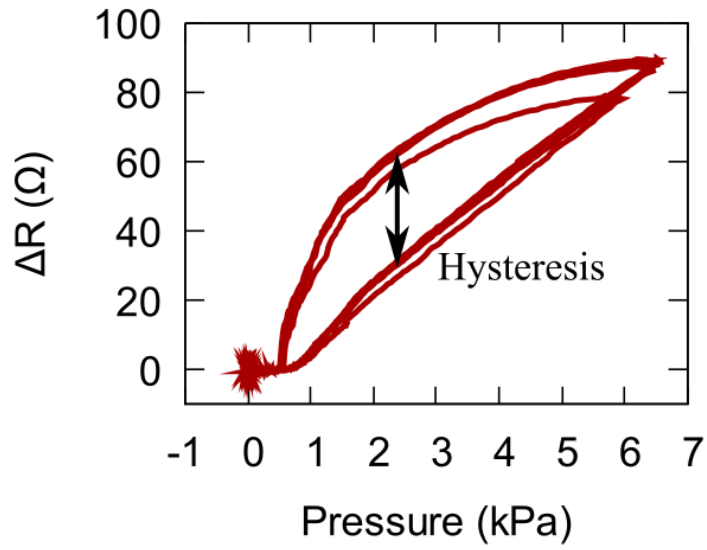
Fig. 6. (a) Sensor resistance responding to loading and unloading of pressure before injection of additional EGaIn (b) after injection of addition EGaIn exhibiting reduced hysteresis
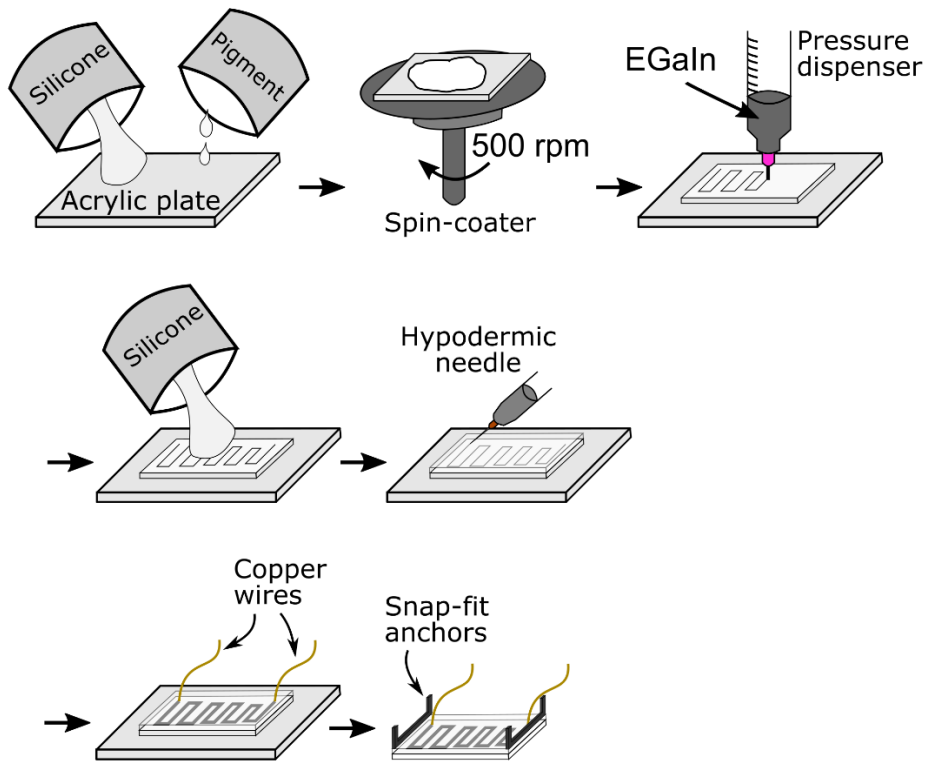
Fig. 7. Fabrication process of the soft tactile sensor using a spin-coater, pressure dispenser, and snap-fit anchors.

3.2. Design of Stretchable Tactile Sensor

Our soft tactile sensor microchannel pattern design is composed of straight horizontal and vertical lines alternating in a serpentine manner [see Fig. 8]. This pattern was chosen because a single straight microchannel pattern deforms in two different manners when stretched along the longitudinal direction and the lateral direction. When stretched vertically, the vertical microchannel patterns increase in length and decrease in cross-sectional area, effectively increasing the resistance of the liquid metal path; the horizontal microchannel patterns, however, decrease in length while the cross-sectional area does not vary drastically, effectively decreasing the resistance of the liquid metal path. Depending on the ratio of the horizontal to vertical microchannel patterns, the electrical resistance of the liquid metal through the entire path increases, decreases, or in a particular case, remains constant as the sensor is stretched. While in other applications the dependence of the microchannel resistance to strain is useful, the purpose of having tactile sensors for our gripper is to be able to detect contact pressures. As a result, the ideal sensor design is one where the resistance is invariant to the strain of the sensor, decoupling the sensor signal to respond only to external pressure.

To obtain such a pattern, sensor microchannel designs with different horizontal to vertical channel length ratios were chosen. Fig. 8(a) lists the seven microchannel design candidates, each having different horizontal to vertical channel length ratios from 1:1 to 7:1.

Sensors of each design candidate were fabricated using EGaIn as the liquid metal conductor embedded inside hyper－elastic silicone rubber (Ecoflex 00－30, Smooth－On) with dimensions of 16 mm by 26 mm and a thickness of 2.4 mm [see Fig. 8]. Fabricated sensors were then attached to a motorized tensile tester (ESM 303, Mark－10) where the electrical resistances of the sensors were measured with a sampling rate of 860 Hz (ADS1118, Texas Instruments) during vertical strain cycles from 0% to 100% at a strain rate of 0.5 mm/min without any external pressure loads. Moving averages of the most recent 30 samples were normalized by the unstrained sensor resistance and plotted for strain in Fig. 8(a). The electrical resistance of the sensor with a 1:1 microchannel length ratio increased the most by 3.5%, whereas the sensor with a 7:1 ratio decreased by roughly 4%. Among the design candidates, the sensor with a 4:1 ratio showed the most insensitive to strain, maintaining less than 1% normalized resistance change throughout the entire 100% strain cycle. By choosing this microchannel pattern ratio for tactile sensors of our gripper fingers, the sensor resistance offsets from finger elongation motions are made insignificant by design for the unloaded state (i.e. no external contact pressure loads).
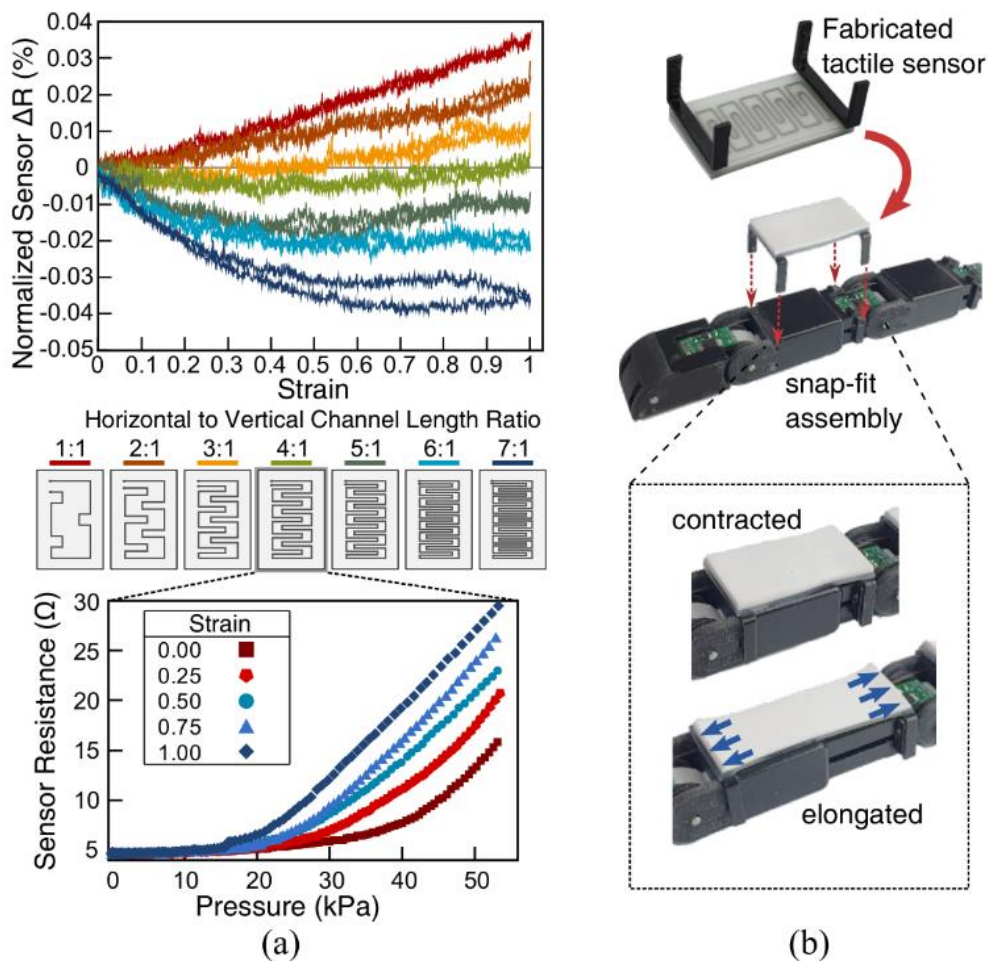
Fig. 8. (a) Normalized changes in sensor resistance vs. strain for seven designs with different horizontal to vertical channel length ratios illustrated below the graph on the top. Sensor resistance vs. pressure for the chosen design with a channel length ratio of 4:1 on the graph below. (b) Fabricated tactile sensor with anchors used for a snap-fit assembly. Contracted and elongated states of the finger with assembled sensor shown underneath.

3 0

3.3. Sensor Characterization and Assembly

Sensor signals according to applied contact pressures for the 4:1 channel length ratio are shown in the bottom graph of Fig 8(a). A commercial load cell (Nano17, ATI Industrial Automation) was attached to the same tensile tester (ESM 303, Mark-10) as above and lowered at 0.5 mm until peak forces of 12 N were reached in the load cell. Sensor signals were received in the same manner as described above throughout the loading process. To measure the resistances at five different sensor strains, the sensor was mounted on a custom-made elongation stage that stretched and anchored the sensor in place. The resistance always increased with increasing contact pressure, but the gain of the signal changes depending on the amount of elongation: increasingly larger gains were observed with increasing strain. Consequently, the sensor responded more sensitively to lower contact pressures at larger strains.

Fig. 8(b) shows the fabricated soft tactile sensor with attached anchors made of an ultraviolet (UV)-cured resin (Veroblack Plus, Stratasys) using a commercial three-dimensional (3D) printer (Objet 30, Stratasys). The anchors were assembled to both ends of the rectangular prism slots by a snap-fit mechanism. Thin enamel-coated copper wires were inserted into the ends of the liquid metal microchannel path and soldered to analog inputs of a custom-made data acquisition (DAQ) board attached at the base of the links near the revolute joints. The elongatable finger with assembled stretchable tactile sensors is shown in both the contracted and

elongated states in Fig. 8(b).

Chapter 4. Control and Manipulation

4.1. Control and Hardware and Setup

The motor control circuits were designed as four identical boards, each with an ARM-based microcontroller (STM32F405RGT6, STMicroelectronics) running at a clock speed of 72 MHz responsible for operating two DC motors through a dual H-Bridge motor driver (DRV8848, Texas Instruments) and tracking encoder positions, collecting sensor signals through a serial protocol interface (SPI), and communicating with other boards through a common controller area network (CAN) bus. One of the boards is responsible for controlling only the motor for abduction/adduction motions, connects to and distributes power from an external power supply of 12 V, and communicates with a computer through a serial bus for positional commands and data logging [see Fig. 9].
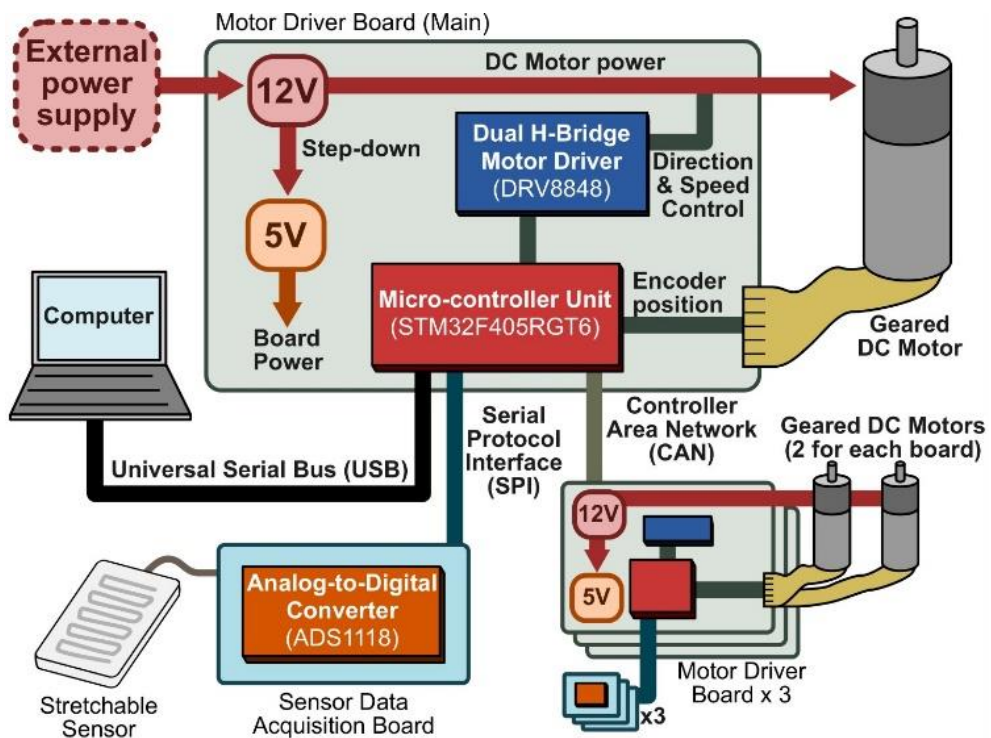
Fig. 9. Motor driver and sensor data acquisition board setup used in control hardware

4.2. Position-control Performance of the Gripper

To evaluate the grasping performance of the gripper for objects of varying size and shape, plastic cylinders fabricated using a commercial 3D printer (Single Plus, Cubicon) of 100 mm, 140 mm, 180 mm in diameter were placed upright on a flat surface. The gripper was attached to the end-effector of a commercial robot arm (UR5, Universal Robots). Initial gripper configuration was set with the three fingers fully extended (largest joint angle sum) but fully contracted (smallest link length sum). After bringing the gripper palm toward the cylinder until contact, the three tendon pair length differences were increased until the joint angle sums became less than the sum of the angles of a polyline corresponding to the finger configuration circumscribing the cylinder. This process was repeated for the most contracted and elongated states, where the link length sums were kept uniform for all three fingers. Position control of the gripper is done in a feedforward manner as the finger joint angles and the link lengths are not measured in real-time.

Depending on the cylinder diameter and the finger lengths, the gripper either was able to obtain a stable grasp on the cylinder or fail to do so by pushing the cylinder away. Fig. 10(a) and (b) show the results for grasping of the 140 mm diameter cylinder at the contracted and the elongated states, respectively, where the former failed at grasping while the latter succeeded. Since the condition for form closure around a cylinder is a grasp that spans over at least half of the circumference, longer link lengths were advantageous over

shorter link lengths in grasping cylinders with larger diameters.

From underactuation, the fingers wrap around the cylinder's surface in a manner that equally distributes the contact force along each link, which helps maximizing the contact span of the grasp in a sweeping grasp. The wrapping of the fingers is observed from the sequential turning of the joint angles as well as from the graph showing the distribution of the cumulative joint angle sum across each individual revolute joint in Fig. 10(b). In a successful grasp, individual joint angles increase in order of the proximal to the distal phalanx until coming in contact with the cylinder. When there is no object to grasp, the proximal joint angle occupies nearly all of the input angle sum, increasing with the tendon length difference [see Fig. 10(c)]. In application, this produces a sweeping motion of the finger during flexion that encourages finger wrapping.

While long finger lengths are advantageous in grasping larger objects, the elongated configurations result in high aspect ratios of the fingers, which is not favorable in grasping smaller objects. Since finger widths are kept the same, the gaps between fingers grow larger with elongation, providing regions through which small objects may fall out during the grasping motion. Adjustment of the finger lengths according to the target object dimensions therefore improves the gripper performance by making use of the more advantageous length configuration during the grasp.

To demonstrate, the gripper was used to grasp a plastic ball of spherical shape with a diameter of 73 mm placed on a small stand on

top of a flat surface [see Fig. 11]. The robot arm was configured such that the gripper palm was parallel to and faces down toward the flat surface from above. First, the fingers were either fully elongated or fully contracted at initial joint angles that allow the fingers to be extended wider than the plastic ball. The gripper was then lowered toward the flat surface until the tip of the fingers were below the plastic ball, after which the fingers were simultaneously flexed in an attempt to grasp the ball. Depending on the finger lengths, the ball either fell out of the gripper or remained in contact with the fingers until a stable grasp was achieved. Fig. 11 shows that contraction of the fingers resulted in a successful grasp, while the same grasping task failed with elongated fingers.
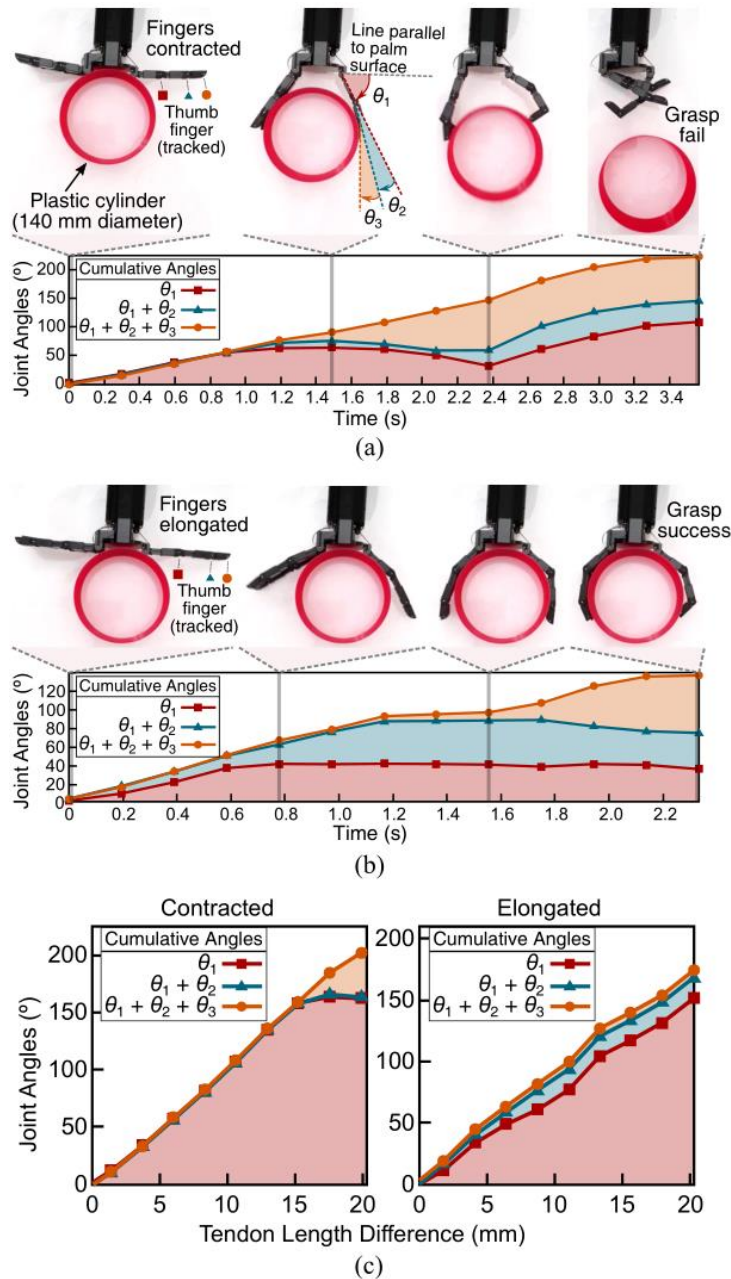
Fig. 10. Grasping a cylinder of 140 mm in diameter with fingers (a) contracted, resulting in a failed grasp, and (b) elongated, resulting in a successful grasp. Individual joint angles are shown cumulatively in the graph below. Vertical bars indicate the instances for the snapshot images above. (c) Cumulative plots of the individual joint angles at contracted and elongated states.

Fingers contracted

Plastic ball
(73 mm diameter)   Mount
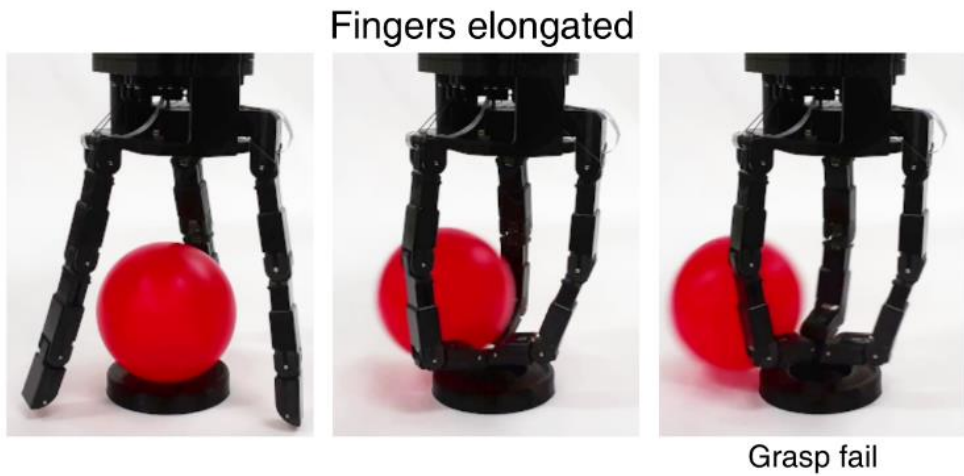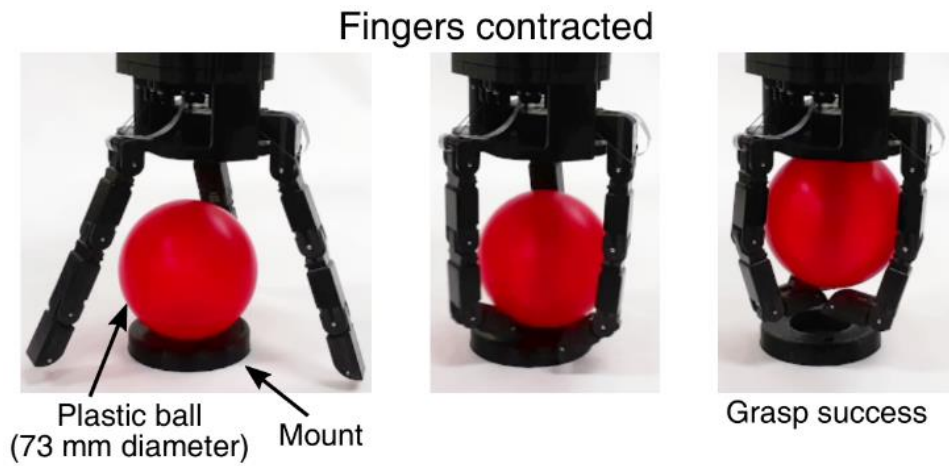
Grasp success

Fingers elongated

Grasp fail

Fig. 11. Grasping a ball of 73 mm in diameter. Successful grasping with contracted fingers on the top, and failed grasping with elongated fingers on the bottom.

4.3. Force-control Performance of the Gripper

Attaching the soft hyper-elastic tactile sensors on the elongatable gripper fingers provides contact pressure information that is used in a force-feedback closed loop control scheme. A typical example of using force-feedback control in grasping is controlling the finger configurations to achieve and maintain a desired contact force range, ensuring that the gripper does not lose the grasp on the target object while also preventing mechanical failures of objects that are soft or brittle.

Our gripper fingers have two independently controllable modes: flexion (joint angle sum) and elongation (link length sum). Either or both of these may be used in the closed-loop control scheme for maintaining a desired contact force. We demonstrate force control using the flexion and elongation modes separately for the grasp of an off-the-shelf rubber balloon that dynamically changes in size during inflation [see Fig. 13]. Based on the readings of the tactile soft sensors, the finger joint angle sums [Fig. 13(a)] and the link length sums [Fig. 13(b)] were controlled to maintain a desired contact pressure of the balloon [see Fig. 12]. Each finger had three sensors attached, one on each of the phalanx (proximal close to the palm, middle in-between, and distal at the fingertip), from which resistance readings were acquired at around 90 Hz. The average of the three sensor signals was used in the feedback loop. As the balloon inflated and increased in size, the contact pressure on the fingers increased as seen in the first half of the sensor graphs in Fig. 13. To relieve

contact pressure, either the joint angle sums were reduced by reducing the tendon length difference (flexion mode control) or the link length sums were increased by increasing the tendon length sum (elongation mode control) as seen in the upper graphs of Fig. 13(a) and (b), respectively. Upon changing the finger configurations accordingly, the contact pressures dropped and maintained a desired average value range as seen in the latter parts of the sensor graphs.
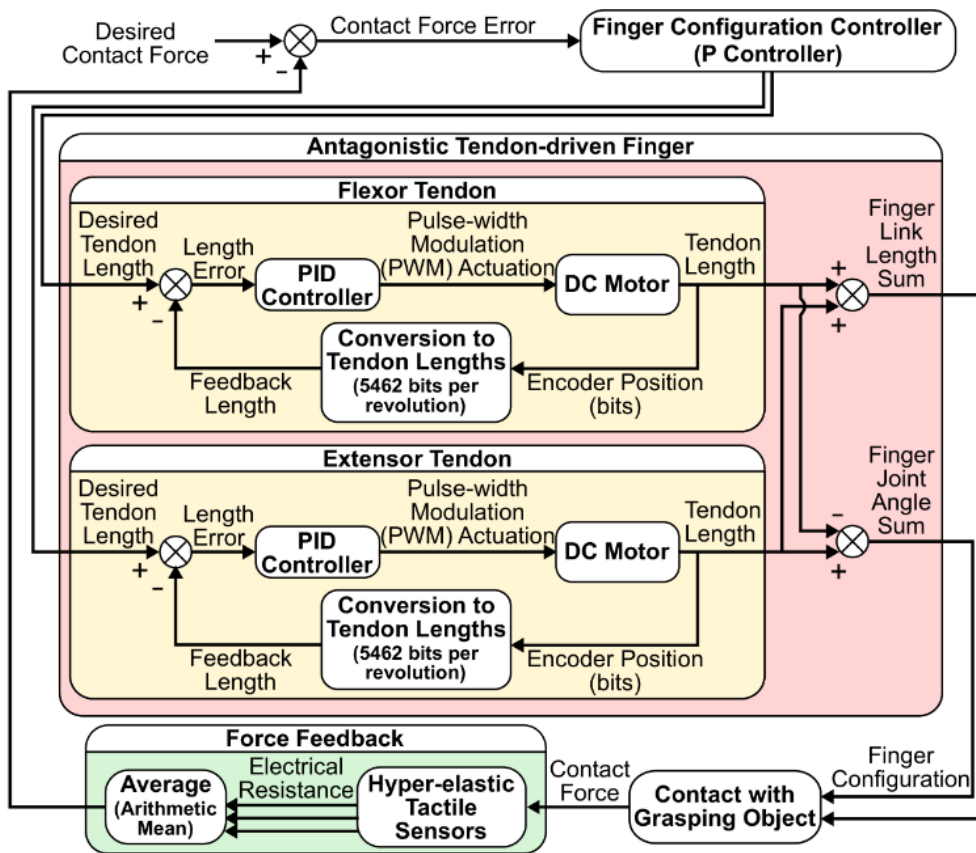
Fig. 12. Schematic diagram of closed loop control for gripper manipulation.

Fig. 13 (a). Grasping a balloon that dynamically changes in size. Plots of the tendon length differences and the tactile sensor readings of each finger are shown underneath, where average values of the sensor readings are indicated by the dashed lines and vertical bars indicate the instances of the snapshots shown above. Gripper fingers are controlled using finger joint angle sums.

4 3

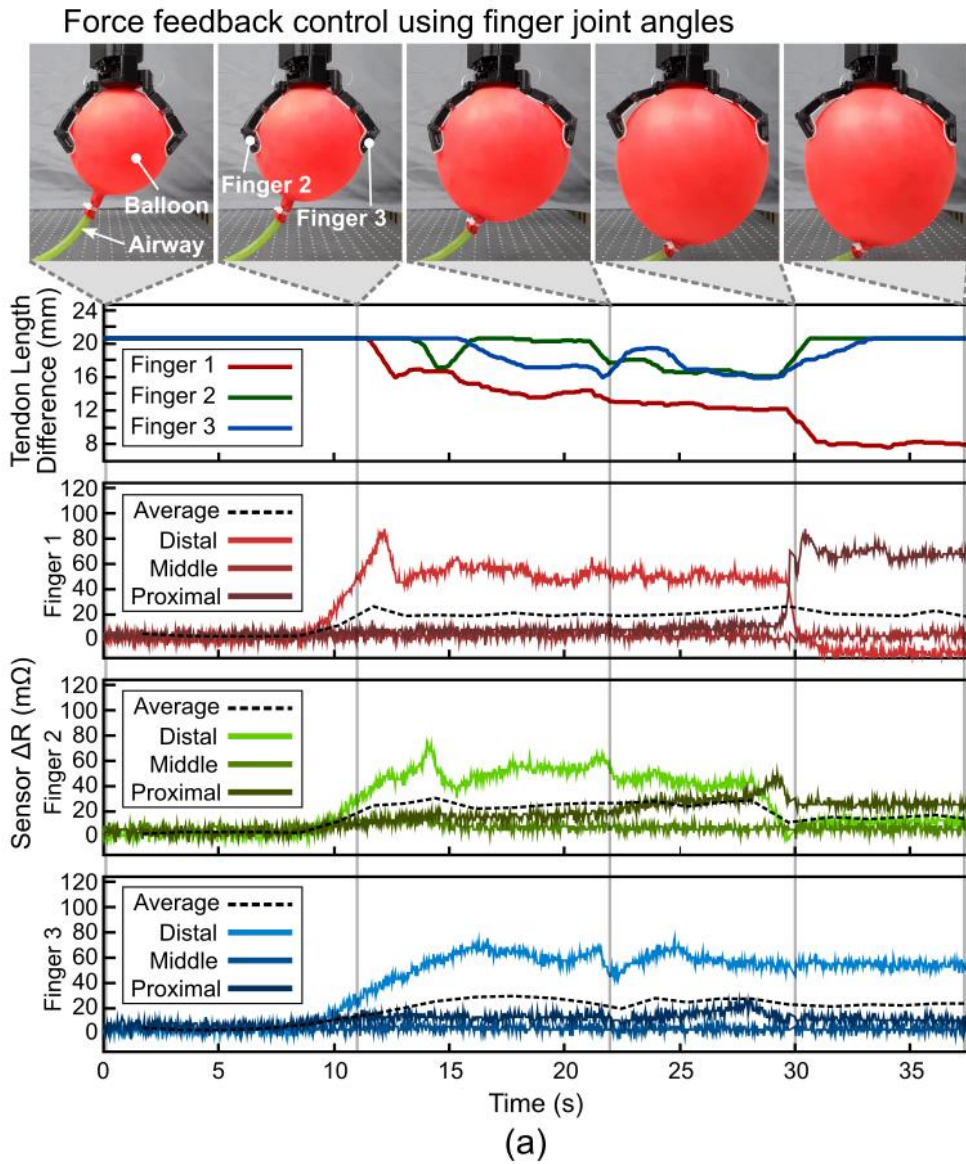**Force feedback control using finger link lengths**
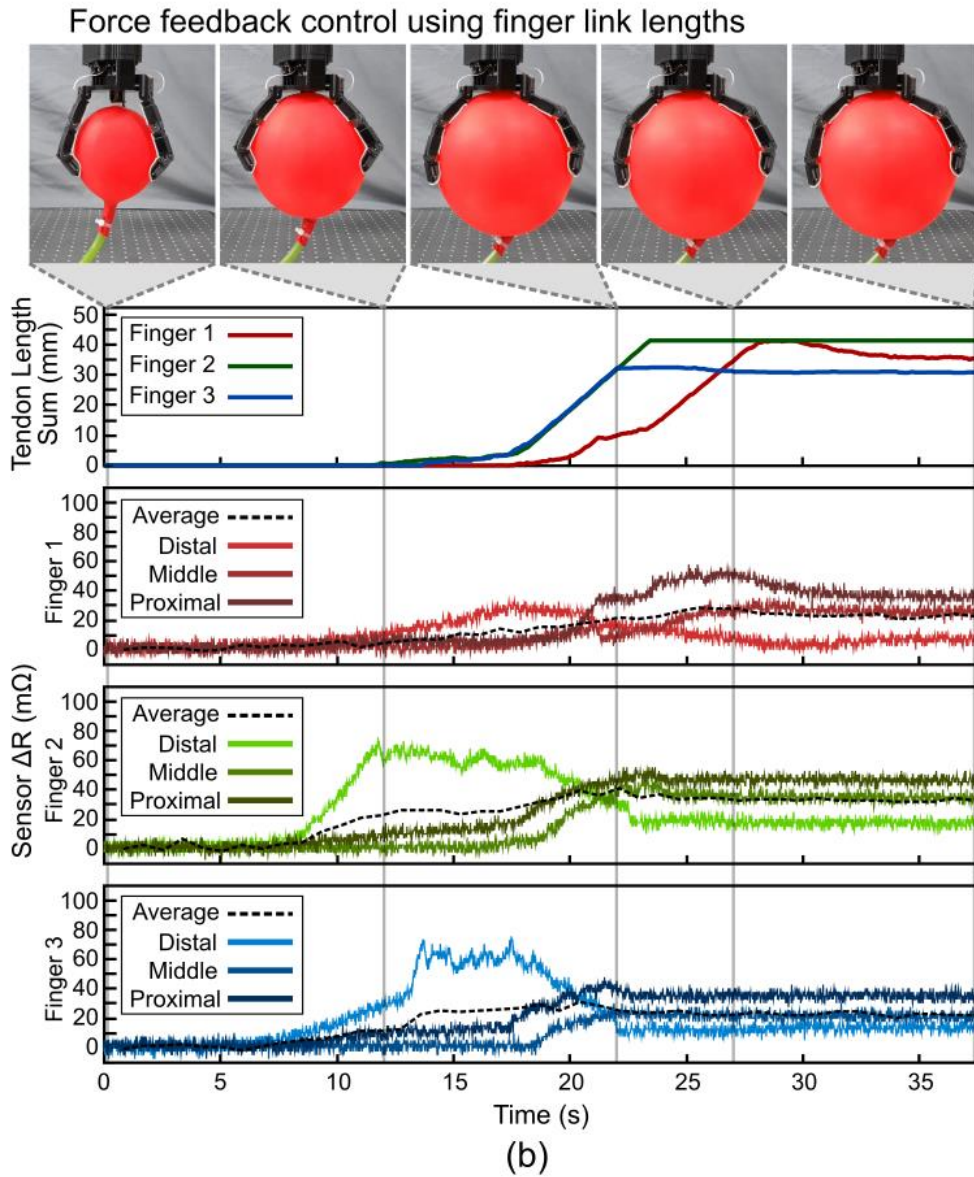
Fig. 13 (b). Grasping a balloon that dynamically changes in size. Plots of the tendon length differences and the tactile sensor readings of each finger are shown underneath, where average values of the sensor readings are indicated by the dashed lines and vertical bars indicate the instances of the snapshots shown above. Gripper fingers are controlled using finger link length sums.

4.4. Multimodal Manipulation

It is also possible to implement a control scheme that utilizes both flexion and elongation modes of the fingers to create motions that are otherwise difficult to generate when using only one of the two. Particularly in the case of using underactuation, having more diverse modes of manipulation improves gripper dexterity since the unactuated DOFs are not controllable. For example, while sweeping grasps using underactuated gripper fingers produces normal contact forces on the object surface, it is difficult to apply tangential forces by only controlling flexion in underactuated grasping. In order to do so, more complex control schemes involving using either the fingertips or pre-calculated motion trajectories are required.

However, introducing elongation to the fingers and combining finger length control with flexion enable the gripper to apply tangential forces to the surface of the grasped object without overly complicating the control scheme. A cylindrically shaped object, for instance, can be turned in place from tangential forces applied on its surface by a gripper finger that first grasps the object using underactuated flexion and then elongates its links. Since the links of the finger will have made contact with the object after the flexion grasp, elongating these links will generate tangential forces at the points of contact.

Multimodal manipulation (elongation and flexion) was demonstrated for a task of opening a bottle cap using our underactuated elongatable gripper, shown in Fig. 14. Two fingers of

the gripper were used to first grasp the bottle to hold it in place using flexion, after which the third finger wrapped around the bottle cap by also using flexion. After the finger made contact with the bottle cap, the finger unscrewed the lid by contracting in length to apply tangential forces in the corresponding direction. Extending the finger afterwards allowed the finger to repeat the unscrewing motion sequence three times for the lid to loosen [see the middle row in Fig. 14]. This bottle cap opening task was shown to be successfully completed by pouring out the water contained inside the bottle by rotating the end-effector of the robot arm to which the gripper was attached.
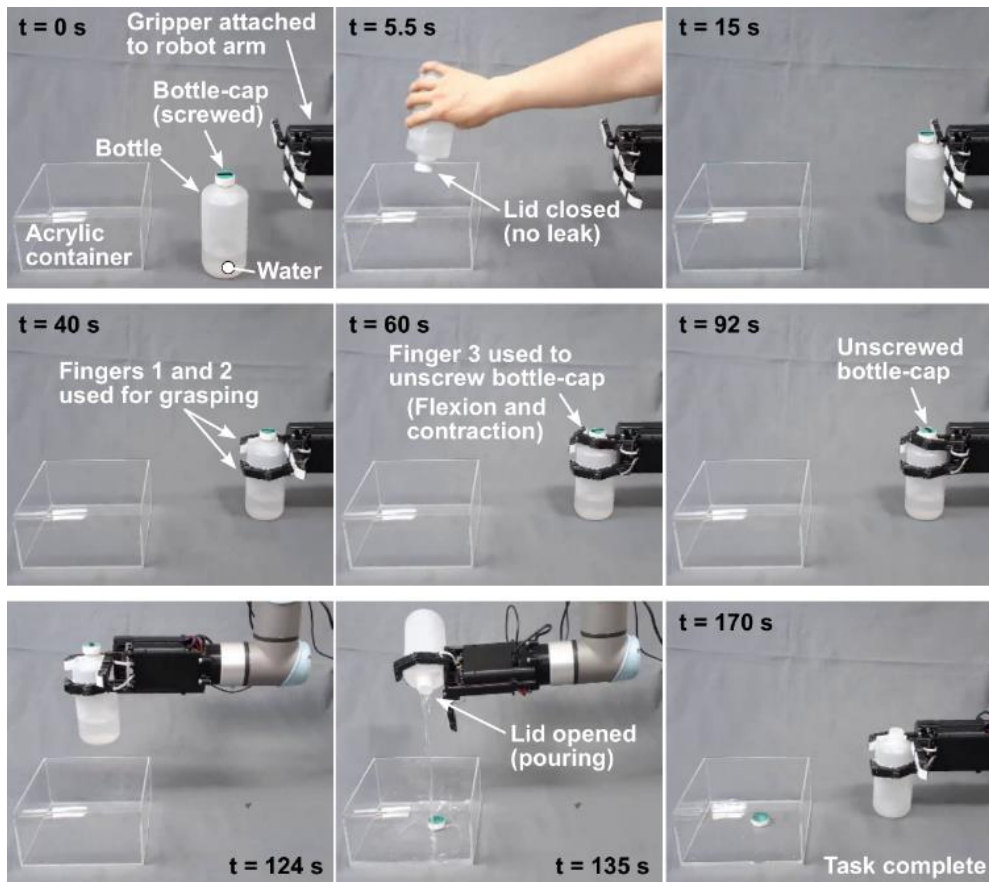
Fig. 14. Bottle-cap opening task in which the gripper fingers are controlled to unscrew the bottle-cap using multimodal manipulation (flexion and elongation). See the supplementary movie.

Chapter 5. Conclusion

While traditional underactuated tendon-driven robot grippers are designed primarily for flexion/extension motions, we have presented a gripper finger design that additionally allows elongation/contraction motions through the use of an antagonistic tendon pair that passes through a serial chain consisting of pulley-tendon-spring modules. The modules were fabricated using revolute joints as pulleys and prismatic joints as rectangular prism slots. Through a geometric model, the relationship between the tendon lengths of our underactuated elongatable finger design to the finger link lengths and joint angles was found and simplified to an intuitive form by unifying the pulley radii of the modules. Based on this design, a finger with three modules (one with a fixed length) was fabricated and characterized using results from the geometric model. Although the finger link length sum and the joint angle sum were not found to be completely decoupled from each other as inferred from the geometric model, finger configurations closely resembled the model's results.

As expected, finger task space increased with elongation; the ability to elongate and contract the fingers improved the grasping performance of the gripper as it extended the size range of graspable objects. By attempting to grasp a plastic cylinder at two different length states, the experiment showed that elongating the fingers for the grasp succeeded while contracting them did not. However, in the case of grasping a smaller spherical ball object, the gripper

performed better when the fingers were contracted. Therefore, controlling the gripper finger lengths appropriately depending on the target object dimensions improved the performance of the grasp. In other words, the ability to elongate or contract the fingers allowed our gripper to grasp a wider variety of objects.

Tactile sensing, while important in grasping and gripper manipulation, is difficult to integrate with our elongatable finger design because traditional tactile sensors are not compatible with large strains. However, soft sensors that use liquid metal microchannels embedded inside hyper−elastic silicone rubber for pressure detection functioned consistently without failure even while stretched, making them compatible with our elongatable finger design. We designed a microchannel pattern that was relatively insensitive to strain and fabricated sensors to assemble with our elongatable fingers.

Using sensor information, force feedback control was implemented in maintaining a desired contact pressure with an inflating balloon. Since our fingers are elongatable, the feedback control can be applied to the finger joint angles, to the link lengths, or to both. Combining the manipulation of elongation and flexion modes of the finger was useful in generating more complex trajectories without overly complicating control, as shown with the bottle cap unscrewing task that used two fingers to grasp the bottle and the third to apply tangential force on the side surface of the lid. The ability of elongating the gripper fingers therefore provides another aspect of

manipulability that adds to the dexterity of the gripper.

Our gripper finger design, however, used springs to maintain tension in the tendon cables and was therefore unable to withstand external forces directed toward the axes of the rectangular prism slots. Use of stiffer compression springs reduces the susceptibility to the displacements resulting from such forces, but does so at the cost of requiring higher tensions of both tendon cables. Larger elongations in the finger design may be considered in future revisions but are still limited to the maximum endurable strains of the attached tactile sensors. For future revisions, designs with higher DOFs will be explored with varying module count, as well as gripper control schemes for carrying out other specific tasks. The ability of finger elongation can be also applied to areas other than the gripper fingers, such as the wrist or the arm, which is expected to improve overall manipulation in application environments.

Bibliography

[1] Firouzeh, A. & Paik, J. Grasp mode and compliance control of an underactuated origami gripper using adjustable stiffness joints. Ieee/asme Transactions on Mechatronics 22, 2165−2173 (2017)

[2] Della Santina, C., Piazza, C., Grioli, G., Catalano, M. G. & Bicchi, A. Toward dexterous manipulation with augmented adaptive synergies: The pisa/iit softhand 2. IEEE Transactions on Robotics 34, 1141−1156 (2018)

[3] Catalano, M. G., Grioli, G., Farnioli, E., Serio, A., Piazza, C. & Bicchi, A. Adaptive synergies for the design and control of the Pisa/IIT SoftHand. The International Journal of Robotics Research 33, 768−782 (2014)

[4] Laliberté, T. & Gosselin, C. M. Simulation and design of underactuated mechanical hands. Mechanism and machine theory 33, 39−57 (1998)

[5] Laliberte, T., Birglen, L. & Gosselin, C. Underactuation in robotic grasping hands. Machine Intelligence & Robotic Control 4, 1−11 (2002)

[6] Amend, J. R., Brown, E., Rodenberg, N., Jaeger, H. M. & Lipson, H. A positive pressure universal gripper based on the jamming of granular material. IEEE transactions on robotics 28, 341−350 (2012)

[7] Tawk, C., Gillett, A., in het Panhuis, M., Spinks, G. M. & Alici, G. A 3D−printed omni−purpose soft gripper. IEEE Transactions on Robotics 35, 1268−1275 (2019)

[8] Kim, W., Byun, J., Kim, J. K., Choi, W. Y., Jakobsen, K., Jakobsen, J., ... & Cho, K. J. Bioinspired dual-morphing stretchable origami. Science Robotics 4 (2019)

[9] Wang, Z., Chathuranga, D. S. & Hirai, S. 3D printed soft gripper for automatic lunch box packing. IEEE International Conference on Robotics and Biomimetics, 503-508 (2016)

[10] Shimojima, H., Yamamoto, K. & KAWAKITA, K. A study of grippers with multiple degrees of mobility: Vibration, control engineering, engineering for industry. JSME international journal 30, 515-522 (1987)

[11] Rojas, N., Ma, R. R. & Dollar, A. M. GR2 gripper: An underactuated hand for open-loop in-hand planar manipulation. IEEE Transactions on Robotics 32, 763-770 (2016)

[12] Bircher, W. G., Dollar, A. M. & Rojas, N. A two-fingered robot gripper with large object reorientation range. IEEE International Conference on Robotics and Automation, 3453-3460 (2017)

[13] Shirafuji, S., Ikemoto, S. & Hosoda, K. Development of a tendon-driven robotic finger for an anthropomorphic robotic hand. The International Journal of Robotics Research 33, 677-693 (2014)

[14] Aukes, D. M., Heyneman, B., Ulmen, J., Stuart, H., Cutkosky, M. R., Kim, S, ... & Edsinger, A. Design and testing of a selectively compliant underactuated hand. The International Journal of Robotics Research 33, 721-735 (2014)

[15] Stuart, H. S., Wang, S. & Cutkosky, M. R. Tunable contact conditions and grasp hydrodynamics using gentle fingertip suction.

IEEE Transactions on Robotics 35, 295-306 (2018)

[16] Aukes, D., Kim, S., Garcia, P., Edsinger, A. & Cutkosky, M. R. Selectively compliant underactuated hand for mobile manipulation. IEEE International conference on robotics and automation, 2824-2829 (2012)

[17] King, J. P., Bauer, D., Schlagenhauf, C., Chang, K. H., Moro, D., Pollard, N. & Coros, S. Design. fabrication, and evaluation of tendon-driven multi-fingered foam hands. IEEE-RAS 18th International Conference on Humanoid Robots, 1-9 (2018)

[18] Bauer, D., Bauer, C., King, J. P., Moro, D., Chang, K. H., Coros, S. & Pollard, N. Design and Control of Foam Hands for Dexterous Manipulation. International Journal of Humanoid Robotics 17, 1950033 (2020)

[19] Odhner, L. U., Jentoft, L. P., Claffee, M. R., Corson, N., Tenzer, Y., Ma, R. R., ... & Dollar, A. M. A compliant, underactuated hand for robust manipulation. The International Journal of Robotics Research 33, 736-752 (2014)

[20] Wang, S., Jiang, H., Myung Huh, T., Sun, D., Ruotolo, W., Miller, M., ... & Cutkosky, M. R. Spinyhand: Contact load sharing for a human-scale climbing robot. Journal of Mechanisms and Robotics 11 (2019)

[21] Dong, H., Asadi, E., Qiu, C., Dai, J. & Chen, I. M. Grasp analysis and optimal design of robotic fingertip for two tendon-driven fingers. Mechanism and Machine Theory 130, 447-462 (2018)

[22] Rossi, C., Savino, S., Niola, V. & Troncone, S. A study of a

robotic hand with tendon driven fingers. Robotica 33, 1034 (2015)

[23] Dong, H., Asadi, E., Qiu, C., Dai, J. & Chen, I. M. Geometric design optimization of an under-actuated tendon-driven robotic gripper. Robotics and Computer-Integrated Manufacturing 50, 80-89 (2018)

[24] Pollard, N. S. & Gilbert, R. C. Tendon arrangement and muscle force requirements for human-like force capabilities in a robotic finger. IEEE International Conference on Robotics and Automation 4, 3755-3762 (2002)

[25] Hazard, C., Pollard, N. & Coros, S. Automated Design of Robotic Hands for In-Hand Manipulation Tasks. International Journal of Humanoid Robotics 17, 1950029 (2020)

[26] Ho, V. & Hirai, S. Design and analysis of a soft-fingered hand with contact feedback. IEEE Robotics and Automation Letters 2, 491-498 (2016)

[27] Baril, M., Laliberte, T., Gosselin, C. & Routhier, F. On the design of a mechanically programmable underactuated anthropomorphic prosthetic gripper. Journal of Mechanical Design 135 (2013)

[28] Ciocarlie, M., Hicks, F. M., Holmberg, R., Hawke, J., Schlicht, M., Gee, J., ... & Bahadur, R. The Velo gripper: A versatile single-actuator design for enveloping, parallel and fingertip grasps. The International Journal of Robotics Research 33, 753-767 (2014)

[29] Maekawa, H., Yokoi, K., Tanie, K., Kaneko, M., Kimura, N. & Imamura, N. Development of a three-fingered robot hand with stiffness control capability. Mechatronics 2, 483-494 (1992)

[30] O'Brien, K. W., Xu, P. A., Levine, D. J., Aubin, C. A., Yang, H. J., Xiao, M. F., ... & Shepherd, R. F. Elastomeric passive transmission for autonomous force-velocity adaptation applied to 3D-printed prosthetics. Science Robotics 3 (2018)

[31] Lee, Y. T., Choi, H. R., Chung, W. K. & Youm, Y. Stiffness control of a coupled tendon-driven robot hand. IEEE Control Systems Magazine 14, 10-19 (1994)

[32] Al Abeach, L. A., Nefti-Meziani, S. & Davis, S. Design of a variable stiffness soft dexterous gripper. Soft robotics 4, 274-284 (2017)

[33] Inoue, T., Yamamoto, S., Miyata, R. & Hirai, S. Robotic joint design by agonist and antagonist arrangement with twisting small-diameter round-belts. IEEE/RSJ International Conference on Intelligent Robots and Systems, 1751-1756 (2015)

[34] Ham, K., Han, J. & Park, Y. J. Soft gripper using variable stiffness mechanism and its application. International Journal of Precision Engineering and Manufacturing 19, 487-494 (2018)

[35] Sujan, V. A. & Dubowsky, S. Design of a lightweight hyper-redundant deployable binary manipulator. J. Mech. Des.126, 29-39 (2004)

[36] Chen, X., Guo, Y., Duanmu, D., Zhou, J., Zhang, W. & Wang, Z. Design and modeling of an extensible soft robotic arm. IEEE Robotics and Automation Letters 4, 4208-4215 (2019)

[37] Schenk, M., Viquerat, A. D., Seffen, K. A. & Guest, S. D. Review of inflatable booms for deployable space structures: packing and

rigidization. Journal of Spacecraft and Rockets 51, 762-778 (2014)

[38] Kim, S. J., Lee, D. Y., Jung, G. P. & Cho, K. J. An origami-inspired, self-locking robotic arm that can be folded flat. Science Robotics 3 (2018)

[39] Ward-Cherrier, B., Cramphorn, L. & Lepora, N. F. Tactile manipulation with a TacThumb integrated on the open-hand M2 gripper. IEEE Robotics and Automation Letters 1, 169-175 (2016)

[40] Park, Y. L., Ryu, S. C., Black, R. J., Chau, K. K., Moslehi, B. & Cutkosky, M. R. force-sensing end-effectors with embedded optical fiber-Bragg-grating sensors. IEEE Transactions on Robotics 25, 1319-1331 (2009)

[41] Drimus, A., Kootstra, G., Bilberg, A. & Kragic, D. Design of a flexible tactile sensor for classification of rigid and deformable objects. Robotics and Autonomous Systems 62, 3-15 (2014)

[42] Park, J. J. & Kim, G. S. Development of the 6-axis force/moment sensor for an intelligent robot's gripper. Sensors and Actuators A: Physical 118, 127-134 (2005)

[43] Lee, J. K., Kim, H. H., Choi, J. W., Lee, K. C. & Lee, S. Development of direct-printed tactile sensors for gripper control through contact and slip detection. International Journal of Control, Automation and Systems 16, 929-936 (2018)

[44] Yuan, W., Dong, S. & Adelson, E. H. Gelsight: High-resolution robot tactile sensors for estimating geometry and force. Sensors 17, 2762 (2017)

[45] Rus, D. & Tolley, M. T. Design, fabrication and control of soft

robots. Nature 521, 467−475 (2015)

[46] Park, M., Ohm, Y., Kim, D. & Park, Y. L. Multi−Material Soft Strain Sensors with High Gauge Factors for Proprioceptive Sensing of Soft Bending Actuators. IEEE International Conference on Soft Robotics, 384−390 (2019)

[47] Park, Y. L., Chen, B. R. & Wood, R. J. Design and fabrication of soft artificial skin using embedded microchannels and liquid conductors. IEEE Sensors journal 12, 2711−2718 (2012)

[48] Shin, H. S., Ryu, J., Majidi, C. & Park, Y. L. Enhanced performance of microfluidic soft pressure sensors with embedded solid microspheres. Journal of Micromechanics and Microengineering 26, 025011 (2016)

[49] Park, Y. L., Tepayotl−Ramirez, D., Wood, R. J. & Majidi, C. Influence of cross−sectional geometry on the sensitivity and hysteresis of liquid−phase electronic pressure sensors. Applied physics letters 101, 191904 (2012)

[50] Vogt, D. M., Park, Y. L. & Wood, R. J. Design and characterization of a soft multi−axis force sensor using embedded microfluidic channels. IEEE sensors Journal 13, 4056−4064 (2013)

[51] Shin, G., Jeon, B. & Park, Y. L. Direct printing of sub−30 m liquid metal patterns on three−dimensional surfaces for stretchable electronics. Journal of Micromechanics and Microengineering 30, 034001 (2020)

Abstract

다양한 모양과 형태를 파지하는 능력은 로봇 그리퍼의 성능을 결정짓는 매우 중요한 지표입니다. 물체의 복잡한 형상에 적응하기 위하여 각 자유도를 통해 복잡한 움직임을 구현해야만 합니다. 그러나 각각의 수많은 관절은 제어하는 것은 복잡성을 야기할 뿐만 아니라, 이로 인하여 회전 관절로 구성된 기존 손가락 디자인이 굴곡, 신전 움직임을 구현하는 부족구동 메커니즘이 도입되었습니다. 이 논문에서는 단 두개의 힘줄로 부족구동을 통하여 제어되고, 마디의 길이가 자유자재로 변화하는 손가락을 소개합니다. 본 그리퍼는 작업공간을 확장하기 위하여 손가락을 늘리거나 파지의 정밀도를 위해 손가락 길이를 줄일 수 있습니다. 촉각 감지를 위하여 고탄성 소프트 센서를 사용하여 손가락의 인장과 함께 늘어날 수 있습니다. 접촉 압력은 관절 각도 또는 링크 길이를 조정하는 힘 제어에서 피드백으로 사용되어집니다. 마지막으로, 인장과 굴곡 모드를 결합한 다중 모드 제어 체계가 조작 작업과 함께 시연됩니다.